2-15-2010

Ion microprobe analysis of oxygen isotopes in garnets of complex chemistry

F. Zeb Page
Oberlin College, Zeb.Page@oberlin.edu

Noriko T. Kita

John W. Valley

Ion microprobe analysis of oxygen isotopes in garnets of complex chemistry

F. Zeb Page[1,2], Noriko T. Kita[1], and John W. Valley[1]

[1]Wisc-SIMS
Department of Geoscience
University of Wisconsin – Madison
1215 W. Dayton St.
Madison, WI, 53706, USA

[2]Department of Geology
Oberlin College
52 W. Lorain St.
Oberlin, OH 44074, USA
zeb.page@oberlin.edu
tel: +1 440 775 6701
fax: +1 440 775 8038

REVISED 10/31/09

key words: garnet, oxygen isotopes, SIMS, ion microprobe, Adirondack Mountains, skarn, diffusion

Abstract

Accurate ion microprobe analysis of oxygen isotope ratios in garnet is possible if appropriate standards are employed to correct for instrumental bias, a component of which depends on the cation chemistry of the analyzed mineral. In this study, 26 garnet standards (including 14 new standards) that span the compositional range of pyrope, almandine, grossular, spessartine, and andradite were analyzed repeatedly by ion microprobe to develop a new method of correcting for instrumental bias in garnets. All analyses were normalized to a single master garnet standard (*UWG-2*) before bias from cation composition was considered. Bias due to cation composition in garnet was found to correlate with grossular content in pyralspite garnets and with andradite in ugrandite garnets. Bias is correlated with molar volume in garnets of all compositions in this study. Although this correlation is suitable as a correction scheme for bias, a more accurate correction scheme based on the grossular and andradite compositions of garnet is proposed. This method reproduces the bias of all but one standard to within a range of 0.4‰, an accuracy that is on the same order as the reproducibility (±0.3‰, 2 S.D.) of the master garnet standard *UWG-2*, but that remains an independent source of error. The new correction scheme is used to successfully reproduce laser fluorination analyses along a traverse of a polymetamorphic, zoned skarn garnet from the Adirondack Mountains. While previous analyses were at the mm-scale, the new data resolve a gradient of $\delta^{18}O$ of 2.1‰ over 16 μm. If experimentally derived diffusion coefficients are correct, these new results show that granulite-facies metamorphism was significantly faster than previously assumed and the thermal peak was less than 5 Myr.

1. Introduction

Metamorphism in hydrothermal systems or skarns is often accompanied by radical shifts in fluid composition and temperature over short time scales (e.g., Taylor and O'Neil, 1977; Bowman, 1998). In response to these changes, garnets and other minerals may form oscillatory zoning patterns in their major and trace element chemistry (e.g., Yardley et al., 1991; Jamtveit et al., 1993) as well as their oxygen isotope ratios (e.g., Clechenko and Valley, 2003). These micro-scale chemical and isotopic variations can be used to reconstruct ancient metamorphic fluid regimes. In particular, the oxygen isotope ratio of metamorphic garnet is a powerful tracer of hydrothermal systems because of the strong isotopic contrast between meteoric and most magmatic fluids (Valley, 1986) and the ability of garnet to preserve these ratios because of slow intragranular diffusion (e.g., Coghlan, 1990; Lancaster et al., 2009). However, the scale of isotopic heterogeneity within skarn minerals is generally much smaller that the volume of material required for analysis by conventional methods. Because of this, skarn garnets are an excellent target for oxygen isotope analysis by ion microprobe, and two studies have used single-collector ion microprobes to show that garnets preserve a detailed oxygen isotopic record of hydrothermal fluid history (Jamtveit and Hervig, 1994; Crowe et al., 2001).

The most recent generation of multicollector ion microprobes has allowed significant advances for in situ oxygen isotope analysis both in terms of reduced analysis spot size and in analytical precision. Analyses of minerals with limited cation solid solution, such as zircon and quartz, have improved from ± 2‰ (2 S.D.) on 30 μm diameter pits (e.g., Valley and Graham, 1991) to ± 0.7‰ (2 S.D.) on 20 μm pits (Cavosie et al., 2005) to ± 0.3‰ (2 S.D.) on 10 μm pits (Kelly et al., 2007; Kita et al., 2009; Valley and Kita; 2009). For ultra-small spots

(< 1μm in diameter) Page et al. (2007) attained a precision of ± 2‰ (2 S.D.). The smaller spot sizes and better precision can be attributed to improvements in technology and to refinements in technique, which include tuning and operation of the instrument, sample preparation, and standardization (Kita et al., 2009; Valley and Kita, 2009). For some minerals, including magnetite and hematite, the orientation of the crystal lattice has been shown to affect the instrument bias (Huberty et al. 2009), however, the data reported here show that any such orientation effect is smaller than the grain-to-grain precision of ±0.3‰ that is regularly attained for randomly orientated grains of garnet. Due to the significant instrument bias inherent in ion microprobe analysis (e.g., Shimizu and Hart, 1982), accurate measurements of stable isotope ratios must be empirically corrected by regular and frequent analysis of well-characterized reference material. Because variable cation composition of some minerals or glasses contributes to the instrumental bias (the "matrix effect" or instrumental mass fractionation e.g., Eiler et al., 1997; Valley and Kita, 2009), most ion microprobe studies of oxygen isotope ratios have been confined to phases of limited solid solution (e.g., zircon, quartz, calcite). In addition, many papers that address instrumental bias and propose correction schemes were developed for a previous generation of single-collector ion microprobes that made use of extreme energy filtering with only one collector and relatively low mass resolution (e.g., Hervig et al., 1992; Riciputi and Paterson, 1994; Eiler et al., 1997; Riciputi et al., 1998). Under these conditions, the instrumental bias can be in excess of 50‰ for $\delta^{18}O$. More recently, Vielzeuf et al. (2005a) addressed the issue of bias in a large-radius multicollector ion microprobe, specifically in aluminous Fe^{2+}-Mg-Ca garnets, and developed a new correction scheme to allow relatively accurate analyses of these compositions (± 1-2‰, 30-50μm pits). The instrument bias for these analyses at high mass-

resolution (MRP~2500) and low energy offset was significantly lower, below 7‰. The cation compositional range of the standards introduced by Vielzeuf et al. (2005a) are sufficient to address the instrumental bias in Al-rich Fe^{2+}-Mg-Ca (pyralspite) garnets commonly found in metasedimentary, metamafic, and some igneous rocks. There are several studies that have established oxygen isotope zoning in garnets of these compositions (e.g., Kohn et al., 1993, 1994, 1997; Skelton et al., 2002; Peck and Valley, 2004) and some that have made use of ion microprobe analysis of zoned pyralspite garnets (Vielzeuf et al., 2005a,b; Martin et al., 2006; Lancaster et al., 2009). However, hydrothermal skarn garnets are most commonly Ca-rich with variable Fe^{3+}/Al (ugrandite) and the Vielzeuf et al. (2005a) standard set and correction scheme does not extend to these compositions.

The present study uses new, higher precision analyses by the latest generation multicollector ion microprobe (ims-1280) to examine instrumental bias systematically from 26 garnet standards covering a wide range of solid solution, including more Ca-rich grossular and andradite compositions. This study has three main goals: 1) to increase the range of possible applications of this method; 2) to develop more straightforward, flexible and accurate correction schemes; and 3) to use these methods to place constraints on the rate of oxygen diffusion in garnet. We have applied our new correction procedure in the analysis of an oscillatory-zoned garnet from the Willsboro Mine, a polymetamorphosed garnet-diopside-wollastonite skarn from the Adirondack Mountains, New York, USA, described by Clechenko and Valley (2003).

2. Garnet Standards

In this study, 27 garnet standards were used to evaluate matrix effects in oxygen isotope analysis by ion microprobe (Table 1). All of these standards were evaluated for oxygen isotopic homogeneity by ion microprobe, and for cation homogeneity by electron microprobe (Supplementary Table A). Oxygen isotope ratios were determined by laser fluorination for all new standards, and in some cases existing standards were analyzed as well for comparison to values in the literature. The standards used in this study and their average cation and isotopic compositions and observed isotopic variability are recorded in Table 1; cation compositions are shown in Figure 1; electron microprobe analyses, cation variability and formula calculation are found in Table A, supplementary electronic materials.

Five garnet standards (Fig. 1) from Eiler et al. (1997) provide near-end-member compositions for grossular (*GrsSE*) and spessartine (*SpsSE*) garnets as well as slightly more dilute almandine (*AlmSE* & *AlmCMG*), and one intermediate almandine-pyrope (*UWG-2*) that is an extremely well-characterized standard for laser fluorination analysis of $\delta^{18}O$ (Valley et al., 1995). Vielzeuf et al. (2005a) increased the cation compositional range of ion microprobe garnet standards, particularly along the pyrope-almandine join by including an end-member pyrope from the Dora Maira quartzite (*PypDM*) and five more intermediate compositions (*PypMM, PypAk, PypAA, Bal509,* β*114).* In addition, they included one more standard on the almandine-grossular join (*2B3*). Detailed information on the origins of these standards as well as chemical composition and unit cell dimensions can be found in Vielzeuf et al. (2005a).

In addition to these existing standards, we introduce 6 garnet standards from eclogitic xenoliths in kimberlite with intermediate almandine – pyrope compositions and from 7 to 61 mol % grossular. Standards *13-63-21, 13-62-27, 13-62-29, 13-63-20,* and *13-63-44* were

separated by Dan Schulze from xenoliths found in the Blaauwbosch kimberlite, South Africa (Ford, 1987; Schulze et al., 2003). Standard *R-53* is from an eclogitic xenolith found in the Roberts-Victor kimberlite (Garlick et al., 1971; MacGregor and Manton, 1986). To supplement the grossular-rich standard (*GrsSE*) used by both Eiler et al. (1997) and Vielzeuf et al. (2005a), we introduce three more grossular-rich garnets (*92W-1, 10691, AF749A)* from garnet-diopside-wollastonite skarn metamorphosed to the granulite faces (Willsboro-Lewis skarn belt, Adirondack Mts., Kohn and Valley, 1998). An additional grossular-rich sample, *MexGrs* (Riciputi et al. 1998) was also analyzed but was excluded from the standard set because of numerous inclusions. Finally, to investigate matrix effects on the grossular-andradite join, we include four more standards (*92Lew-2, 92Lew-7, 92Lew-8, 92Lew-10*) with the compositional range $And_{49\text{-}91}$, from the same skarn belt (Kohn and Valley, 1998).

3. Analytical Methods

3.1 Sample Preparation

Garnet standards were crushed by hand, cast in 25 mm epoxy disks, and polished. All garnet standards and samples were mounted within 5 mm of the center of the epoxy disk, and all mounts include multiple grains of the *UWG-2* standard at the center of the mount. Standards vary in grain size from ~150 μm to up to 5 mm, depending on the nature of the source material; between 3 and 36 grains of each standard were mounted in standard blocks. A zoned grossular-andradite garnet from the Willsboro wollastonite skarn (Adirondack Highlands, New York) that was previously analyzed for traverses of $\delta^{18}O$ at mm-scale by laser fluorination (garnet 1a of Clechenko and Valley, 2003) using a thin saw-blade technique (Elsenheimer and Valley, 1993) was also prepared for ion microprobe analysis.

The Willsboro sample consists of a 700 µm thick polished wafer of rock (thick section) attached to a glass microscope slide with superglue from which a ~1 mm wide strip of material that represents a core to rim garnet transect had been removed and analyzed in chips by laser fluorination. The portion of the garnet immediately adjacent to this transect was removed from the slide with acetone and cast in the center of an epoxy disk containing the *UWG-2* standard and repolished for ion microprobe analysis.

3.2 Electron Microprobe

Cation chemistry of garnets was determined using the CAMECA SX51 electron microprobe at the University of Wisconsin - Madison. Garnets were analyzed in point beam mode with an accelerating potential of 15 kV and 20 nA beam current. The counting time was 10s on peak and 5s on both sides, off-peak. Natural and synthetic silicate and oxide standards were used. Data were reduced using the Probe for Windows software (Donovan et al., 2007), and oxygen was calculated by stochiometry. Fe^{2+}/Fe^{3+} was estimated by charge-balance, assuming no site vacancies or OH substitution (Afifi and Essene, 1988). Chemical analyses of all garnet standards are presented in Supplementary Table A and summarized in Table 1.

3.3 Laser Fluorination

Analysis of oxygen isotopes to calibrate ion microprobe analyses for new standard material was performed on 1-2 mg garnet chips that were treated overnight at room temperature in the sample chamber with BrF_5, then individually heated with a CO_2 laser in the presence of BrF_5 to release O_2, which was cryogenically purified, converted into CO_2, and analyzed on a Finnigan MAT 251 mass spectrometer (Valley et al., 1995). Isotopic ratios are reported in per mil (‰) notation relative to standard mean ocean water (VSMOW).

Accuracy and analytical precision were verified during each session by multiple analyses of the garnet standard *UWG-2* (Valley et al., 1995). Raw standard $\delta^{18}O$ values for each session were corrected to the accepted UWG-2 value ($\delta^{18}O$ = 5.80‰ VSMOW) and the same correction was applied to samples. The average uncorrected $\delta^{18}O$ value (± 2 S.D.) of UWG-2 was 5.59 ± 0.08‰ (n=5).

3.4 Ion Microprobe

3.4.1 Analysis Conditions

Oxygen isotopic analyses were performed on the WiscSIMS CAMECA ims-1280 high-resolution, multi-collector ion microprobe at the University of Wisconsin – Madison in 10 analytical sessions over the course of over 2 years. A $^{133}Cs^{+}$ primary ion beam (20 kV total accelerating voltage) was focused to a diameter of 10 µm on the gold-coated sample surface. Secondary O^{-} ions were accelerated away from the sample by –10 kV and the analysis site was centered under a uniform electron field generated by a normal-incidence electron gun for charge compensation. Primary ion intensities were ca. 2-3 nA. The secondary ion optics were configured similarly to those reported in Kita et al. (2009) in order to achieve high secondary ion transmission. Instrument parameters include: transfer lens magnification of 200, contrast aperture (CA) 400 µm diameter, field aperture (FA) 4000 x 4000 µm square, entrance slit width 122 µm, energy slit width 40 eV, and exit slit width 500µm. At these conditions, both the primary ion spot image transferred to the FA window and the crossover image through the CA and entrance slit were almost fully transmitted compared to fully opened conditions. The intensity of ^{16}O was 2 to 3 $x10^{9}$ cps depending on the primary intensity (ca. 10^{9} cps/nA). Mass resolving power (MRP, $M/\Delta M$), measured at 10% peak height, was set to ca. 2200, enough to separate hydride interferences on ^{18}O. Two

185 Faraday cups (FC) were used to measure ^{16}O and ^{18}O simultaneously and the amplifiers on
186 each were equipped with 10^{10} and 10^{11} Ω resistors, respectively. The base line of the FC
187 amplifiers was measured at the beginning of each analytical session; drift during the day was
188 insignificant compared to the noise level of the detectors (≤1000 cps for the ^{18}O FC with 10^{11}
189 Ω resistor, Kita et al., 2009). The magnetic field was regulated by a Nuclear Magnetic
190 Resonance (NMR) probe with stability of mass better than 10 ppm/10 hours. At each analysis
191 position, any small misalignment of the secondary optics due to changing stage position was
192 automatically re-tuned before analysis. Instrument stability during each analytical session is
193 documented by repeated analyses of the UWG-2 standard (Supplementary Table B).
194 *3.4.2 Standardization*
195 Minerals with limited solid solution (e.g., quartz, calcite, zircon) are corrected for
196 instrument bias by adjusting the raw data by a factor ($\alpha^{18}O_{SIMS}$) obtained by analyzing a
197 standard of the same mineral and chemical composition embedded in the same mount.
198 Blocks of typically 4 standard analyses (different spots on one or more grains) are made
199 before and after each set of sample analyses. In order to isolate the variation of bias
200 generated by matrix effects within the garnet family from other sources of bias such as
201 variability of instrument conditions over time, raw data from all garnet analyses (sample and
202 compositional standard) were first corrected using the bracketing analyses of the *UWG-2*
203 standard that is embedded in each sample mount. A fractionation factor ($\alpha^{18}O^*_{SIMS}$) is
204 calculated from the bracketing analyses of *UWG*-2 relative to the accepted value of *UWG-2*
205 on the VSMOW scale (5.80‰, Valley et al., 1995) following equation 2.1 in Kita et al.
206 (2009).
207

$$\alpha^{18}\mathrm{O}^{*}_{SIMS} = \frac{1+\left(\delta^{18}\mathrm{O}_{RAW}/1000\right)}{1+\left(\delta^{18}\mathrm{O}_{VSMOW}/1000\right)} \quad (3.1)$$

A preliminary $\delta^{18}O$ value for each sample (or compositional standard) is then calculated using $\alpha^{18}O^{*}_{SIMS}$ and equation 2.5 of Kita et al. (2009).

$$\delta^{18}\mathrm{O}^{*} = \left\{\left[1+\left(\delta^{18}\mathrm{O}_{RAW}/1000\right)\right]/\alpha^{18}\mathrm{O}^{*}_{SIMS} - 1\right\}\times 1000 \quad (3.2)$$

This preliminary corrected value is denoted as $\delta^{18}O^{*}$ and is the same as $\delta^{18}O_{VSMOW}$ only for garnets with the same bias (or chemical composition) as *UWG-2* and $\delta^{18}O^{*}$ increasingly differs from the VSMOW scale as garnet compositions (and biases) differ from that of *UWG-2*. The use of a preliminary correction to $\delta^{18}O^{*}$ allows comparison of data between standard brackets or between different analysis sessions, but does not take into account the bias generated by chemical variability among garnets. This bias observed in the 25 other (secondary) garnet standards (vs. UWG-2) can be expressed in permil deviation from the bias observed in the analysis of *UWG-2* with the following relation:

$$(\text{bias rel. } UWG\text{-}2) \approx \delta^{18}O^{*} - \delta^{18}O \quad (3.3)$$

where $\delta^{18}O$ is the isotopic composition of the standard on the VSMOW scale as determined by laser fluorination. Because the bias, $\delta^{18}O^{*}$ and $\delta^{18}O$ generally differ by less than 10‰ (and in most cases, they differ by much less) this approximation is accurate to within 0.1‰ (Kita et al. 2009).

For analyses of sample garnets, a correction is applied based on the compositional dependence of bias observed among standards analyzed during the same analysis session. Different possible correction schemes are compared in section 5.4. In addition to isolating compositional effects from other sources of bias, this correction method allows us to use a single, particularly well-characterized standard (*UWG-2*) to evaluate spot-to-spot

reproducibility of analyses by emulating the standard-sample-standard bracketing correction schemes used to ensure high precision and accuracy oxygen isotopic analyses of other phases such as zircon, calcite, and quartz. Finally, using *UWG-2* as a "master standard" allows a significant practical advantage in that only one standard need be embedded in each sample mount, and other standard material used to evaluate or correct for matrix bias can be reused in separate standard mounts as long as they are also corrected to *UWG-2*. The external errors of bracketing *UWG-2* analyses were typically 0.2-0.4‰ (2 S.D.) for 10μm diameter analysis pits. After ion microprobe analysis, the bottoms of all pits were examined by scanning electron microscope in secondary electron imaging for inclusions and cracks that might affect the measured oxygen isotope ratios, and classified as "regular" or "irregular" according to Cavosie *et al.* (2005). All data used in this study are exclusively from pits that were observed to be "regular" (inclusion and crack-free).

3.4.3 Sputter test

Eiler et al. (1997) observed a strong correlation with a single collector ion microprobe between the bias and sputter rate of glasses of various compositions and albite, and used this correlation as the foundation of a kinetic model to predict matrix effect bias. To compare the sputter rate of sample material with instrument bias, we conducted a sputtering rate test on a subset of garnet standards. The primary Cs^+ ion beam was focused into a point beam and rastered over a 30 x 30 μm region for 60 minutes. The dimensions of the pits were measured at nm-scale using a Zygo white-light profilometer. The rastered pits were found to have flat bottoms, and the depth was by taken as the average depth of the center portion of four transects through the center of each square pit. The reproducibility of this measurement was on the order of 2-3 nm for a single pit.

4. Results

Garnet standards were analyzed in ten sessions from April 2006 to August 2008, with between 3 and 25 standards analyzed per session. Each standard was analyzed between 4 and 20 times per session and bias data were corrected by the average bias calculated from the bracketing *UWG-2* analyses. Instrumental bias measured on *UWG-2* ranged from 1.5 to 4.6‰ between analysis sessions, but varied by less than 0.6‰ within a single session (average reproducibility = ±0.3‰ 2 S.D.). Spot to spot reproducibility of secondary standards ranges from ±0.2 to ±0.8‰ (2 S.D.) with an average reproducibility of 0.4‰ (2 S.D., Table 1). More than half of the standards, spanning the entire compositional range, displayed variability on the same order as the analytical uncertainty (≤ 0.4‰, 2 S.D.). The observed variability in a number of standards greater that analytical uncertainty is likely due to some small degree of natural heterogeneity. The bias relative to *UWG-2* for each standard in each session is reported in Table 2, and detailed data from each analysis session can be found in Table B of the electronic supplementary materials. When standards were analyzed multiple times over the 28-month period, bias relative to *UWG-2* was found to vary on average by ±0.3‰ and in all cases less than ±0.7‰.

The component of instrumental bias caused by matrix effects (i.e., bias rel. to *UWG-2*) of garnet standards in this study ranges from -1.1‰ for near end-member pyrope and almandine standards to +7.1‰ for the most andradite-rich standard. Low-Ca (grossular + andradite < 20 mol%) standards (pyrope, almandine, and the single spessartine) have a very limited range of bias (1.5‰) out of the total range of 8.2‰. In Al-rich, Mg-Fe^{2+}-Ca garnets, bias ranges 4‰ (-1.1 to +2.9‰ relative to *UWG-2*) and correlates with the grossular content

(Fig. 2a) as previously described by Vielzeuf et al. (2005a). However, in grossular-andradite garnets bias ranges an additional 4.2‰ (+2.9 to +7.1‰ relative to *UWG-2*) and is inversely correlated with the grossular content (Fig. 2b) and positively correlated with the andradite content. Data from the sputter test are presented in Table C and are plotted in Figure A of the electronic supplementary materials; no correlation was found between sputter rate and bias for garnets, in contrast to single detector data at high energy offset for albite and silicate glasses (Eiler et al., 1997).

5. Discussion

5.1 Comparison with previous work

There is a broad correlation in the magnitude and sign of instrumental biases among standards of similar composition used in this study and Vielzeuf et al. (2005a). However, there are significant differences in the measured bias values between the two studies. The total range in bias varies up to 6.3‰ in Vielzeuf et al. (2005a) but varies only 4.0‰ over the same compositional range in this study. The bias on *UWG-2* ranges between 1.5 and 4.6‰ between analysis sessions in this study, whereas it varies from -4.8 to 0.5‰ in Vielzeuf et al. (2005a). Although the different ranges of UWG-2 values (range = 3.1 vs. 5.3‰) suggests greater variability in instrument conditions in one study, the differences in bias between the two multicollector ion microprobe studies are small when compared with the -60.4‰ bias generated by the analysis of *UWG-2* on a single collector ion microprobe at high energy offset (Eiler et al., 1997). A more detailed comparison between the present study and that of Vielzeuf et al. (2005a) is somewhat confounded by different standardization techniques. Vielzeuf et al. (2005a) did not run a specific standard (such as *UWG-2*) as frequently as in this study to correct for small instrumental drifts and simply reported instrumental bias for

each standard relative to the VSMOW scale. Because of this, measurements of instrumental bias for every garnet standard (*UWG-2* and other standards) within and among analysis sessions include changes in instrumental conditions and may not be directly compared.

5.2 Bias and garnet composition

Instrument bias in garnets is strongly correlated with Ca-content in Al-rich garnets and appears to be approximately linear for compositions of less than ~30 mol.% grossular (Fig. 2a). However, compositions of greater than 30 mol.% grossular affect bias to a lesser degree. Bias changes ~ 2‰ relative to *UWG-2* between 0-30 mol.% grossular, but only increases an additional ~2‰ between 30-90 mol.% grossular. This non-linear relationship between bias and composition is consistent with similar trends observed in feldspars, pyroxenes, olivine, and carbonates (Valley and Kita, 2009) In Ca-rich garnets, bias is inversely correlated with grossular (Al) content (Fig. 2b) and positively correlated with andradite (Fe^{3+}), with one clear outlier (*MexGrs*). The instrumental bias measured for *MexGrs* is consistently > 1‰ greater than the four other grossular-rich garnets of similar composition in this study. Ion microprobe analyses of *MexGrs* suggest that the garnet itself is not strongly variable in oxygen isotopic composition (±0.7‰ 2 S.D.). However, unlike any other garnet in this study, *MexGrs* contains a substantial number of inclusions. Although these inclusions are easy to avoid with the ion microprobe, the calibration by laser fluorination analysis constitutes a mixture of garnet and inclusion material. For this reason we exclude *MexGrs* as a standard material in our calibration, although we show the data for completeness.

Vielzeuf et al. (2005a) recognized a correlation between the Ca content of Al-rich garnets and bias in most of their analysis sessions. This observation is largely based on one

Ca-rich standard (*GrsSE*). The addition of more Ca-rich standards in this study confirms the strong correlation between Ca (grossular) and bias, and indicates that Fe^{+3} (andradite) has an even stronger effect on instrumental bias.

5.3 Bias and molar volume

Andradite and grossular have a substantially larger unit cell dimension than the other garnet end-members in this study. In order to test a correlation between molar volume and instrument bias (a possibility proposed by Vielzeuf et al., 2005a), the molar volume of each garnet standard was estimated as a weighted average of the molar volumes of end-members assuming ideal mixing. Volume data for pyrope, almandine, grossular, and andradite are taken from Robie and Hemingway (1995) and volume data for spessartine and uvarovite are from Diella et al. (2004). Physical properties of garnet such as unit cell dimension have long been successfully approximated from chemical data (e.g., Novak and Gibbs, 1971). The calculated molar volume for each standard can be found in Table 1, and agree well with the molar volumes determined for the subset of standards with published volumes determined by X-ray diffraction (Vielzeuf et al. 2005a).

The instrumental bias for the garnet standards in this study is well correlated with the calculated molar volume (Fig. 3). A least-squares linear regression of the data for all 26 standards (excluding MexGrs) yields an R^2 value of 0.95. However, there is substantial variability of the data about the best-fit line, greater than the degree of observed heterogeneity in both cation and isotopic composition of the garnet standards. As in the study of Vielzeuf et al. (2005a), the lone spessartine-rich standard (*SpsSE*) lies well below the correlation between molar volume and bias line. However, *SpsSE* is not an outlier in the correlation between grossular and bias among Al-rich garnets (Fig. 2a).

Although the correlation between molar volume and bias provides a simple linear relationship, it does not explain the relatively large degree of variability observed among standards of similar cation composition, particularly those rich in grossular (even without *MexGrs*). One possibility in the case of greater observed bias than that predicted by calculated molar volume is the presence of an end-member such as hydrogrossular or hydroandradite that is analytically difficult to measure, but has a strong effect on molar volume. However, there is no evidence of a significant detectable hydrogen-bearing component (in the form of silica deficiency) for any of these standards. Although molar volume may provide a strong control on bias, one or more additional second-order effects may be responsible for the observed variability.

5.4 Correction scheme

Correlations between physical properties and instrumental bias have been reported before (Hervig et al. 1992, Eiler et al. 1997, Riciputi et al. 1998). These workers noted a correlation between atomic mass and bias but also observed that the presence of residuals of up to 10‰ made this correlation unsuitable as a correction scheme. Most recently, Vielzeuf et al. (2005a) reported a correlation between molar volume and bias for garnets. However, because of limited standards, this correlation was deemed unsuitable as the basis for a correction scheme.

With the increased number of standards in this study, the observed correlation between calculated molar volume and bias could be used as a basis for correction. A least-squares linear regression of the data for 25 standards (not including the 2σ *SpsSE)* yields the relation:

Bias (‰ relative to UWG-2) = 0.426 x calc. molar volume (cc/mol) - 49.42 (5.1)

with an R^2 value of 0.97 (2 S.E. of the estimate = 0.88‰). This represents a substantial improvement in comparison to the correction scheme of Vielzeuf et al. (2005a) that was based on a linear interpolation of the bias of four standards that bracket the sample in almandine, pyrope, grossular, and spessartine content. The relation between bias and molar volume described by equation (5.1) reproduces the measured composition of 75% of the 25 standards used to within ±0.5‰ of their accepted value, 85% to within ±0.6‰, and 95% to within 0.7‰. Despite the extension in compositional range offered by this correction scheme, the improvement in accuracy (± 0.88‰ 2 S.E. of the estimate based on 25 garnets) is still substantially worse that the precision of the method as evidenced by typical reproducibility of standard analyses on the order of ±0.4‰ (2 S.D.).

Another possible correction scheme is based on compositional variables, particularly the strong correlation between bias and grossular content in pyralspite garnets and andradite in ugrandite garnets. Riciputi et al. (1998) showed that instrumental bias in grossular-andradite garnets in single-collector ion microprobes could be estimated using a linear interpolation of bias along the Al-Fe^{3+} chemical join, and suggested that this be the basis of a correction scheme. In this study, the relationships between bias and grossular among pyralspite garnets and between bias and andradite in ugrandite garnets are non-linear (Fig. 4). However, both are well-modeled with simple polynomial functions, with far less variability than the linear regression between molar volume and bias. This non-linear relationship is similar to that observed among other silicates and carbonates (Valley and Kita, 2009). The instrumental bias of the nineteen standards with less than 5 mol.% andradite (including *SpsSE*) can be related to the mole fraction of grossular (+minor uvarovite) with the following relation:

391 Bias (‰ relative to UWG-2) = $-5.04(X_{Grs+Uvar})^2 + 8.96(X_{Grs+Uvar}) - 1.09$ (5.2)

392 For the 8 garnet standards (excluding *MexGrs*) that contain less than 10% almandine +
393 pyrope + grossular, bias can be related to andradite (+ minor CaTi garnet) as

394 Bias (‰ relative to UWG-2) = $-1.92(X_{And+CaTi})^2 + 6.18(X_{And+CaTi}) - 2.87$ (5.3)

395 These two calibrations reproduce the actual compositions of the 26 garnet standards used to
396 ± 0.40‰ (2 S.E. of the estimate), a substantial improvement to the molar volume correction
397 that makes accuracy comparable to the reproducibility of most garnet standards.

398 It is important to stress that the calibrations above are presented to demonstrate and
399 compare between methods of correction. The values of instrumental bias measured relative to
400 *UWG-2* for each standard remain remarkably consistent between analysis sessions, but
401 should in no way be the basis for correction of data collected on different instruments under
402 different operating conditions. New calibration curves should be generated by users on their
403 own instruments, ideally during the same analysis session as the samples to be corrected. The
404 use of a calibration based on 26 garnet standards (or even a substantial subset thereof) that
405 need to be analyzed during each analysis session is impractical for routine correction of
406 garnet data. A more practical approach to a correction scheme correction is to use a subset of
407 standards that compositionally bracket the unknown and then estimate bias based on the
408 grossular or andradite composition as appropriate. Our preferred correction procedure is a
409 calibration curve based on grossular or andradite composition. At least 3-4 standards are
410 analyzed that bracket the chemical composition of the unknown sample and delineate the
411 overall shape of the curve (e.g., both low and high grossular/andradite standards are included
412 in each calibration to avoid artifacts that might arise from a quadratic equation fit to only
413 three points over a narrow compositional range). Compositional standards should be

414 analyzed during the same analysis session as samples to be corrected. A number of
415 calibration curves were generated based on 3-4 standards using this approach. As long as the
416 standards were chosen to cover a broad range of grossular or andradite compositions, the
417 calibrations reproduced the full 26 garnet standard set to within ± 0.3-0.5‰ (2 S.E. of the
418 estimate). This approach yields similar accuracy to that achieved with use of all standards.
419 The use of a correction procedure in which all samples are first normalized to *UWG-2*
420 to correct for any instrumental instability and then corrected for matrix effect bias using the
421 grossular or andradite of at least 3 secondary standards that compositionally bracket the
422 unknown offers significant advantages in precision, accuracy, and convenience. Correction to
423 a master standard allows for a single consistent method of determining the precision
424 (reproducibility) of analyses as well as the practical advantage of allowing compositional
425 standards to be stored in standard mounts and not embedded with samples. This allows use of
426 the best and most plentiful standard for all sample mounts, and conserves more precious
427 materials.
428 Errors in ion microprobe analyses arise from a myriad of sources ranging from
429 counting statistics to sample topography (e.g., Kita et al., 2009). Propagation of all these
430 sources of error would be an extremely arduous undertaking, and for this reason the external
431 reproducibility of a standard is the best (and most workable) metric for error estimation
432 (Valley and Kita, 2009). An instrumental bias calibration that is dependant on compositional
433 variables introduces a new source of error independent of that measured by standard
434 reproducibility. Errors resulting from the calibration scheme must therefore be added in
435 quadrature to those arising from analytical uncertainty. However, it should be noted that the
436 proposed calibration does not fully explain all sources of instrumental bias just as counting

statistics do not encompass all other sources of error in an analysis. True statistical rigor in the treatment of these uncertainties is, as yet, impossible.

6. Application to growth zoning and diffusion

6.1 Adirondack skarn garnet

The Adirondack Mountains of New York, USA are a Mid-Proterozoic, polymetamorphic, granulite-facies orogenic terrane. Intrusion of anorthosite and related magmas (1155±5 Ma, McLelland et al., 2004) formed a contact metamorphic aureole including skarn rocks that predate the peak of regional metamorphism (Valley and O'Neil, 1982; Valley, 1985; Valley et al., 1990). The Adirondack skarns were buried and largely recrystallized during the Ottawan (ca. 1050 Ma) regional granulite-facies metamorphism, but small domains of unrecrystallized, oscillatory-zoned skarn garnets were locally preserved at the Willsboro Mine. Clechenko and Valley (2003) analyzed the oxygen isotopic composition of one to two centimeter diameter zoned garnets from Willsboro by laser fluorination of mm-scale chips taken from a core to rim transect of the garnets removed with a thin diamond saw. The oxygen isotopic composition of this transect in combination with major and trace element data were used to infer variable mixing of metamorphic fluids from meteoric (low $\delta^{18}O$, Ca-rich) and magmatic (high $\delta^{18}O$, Fe-rich) sources. The garnet zoning was preserved through subsequent granulite-faces metamorphism.

In this study we analyze oxygen isotope ratios along a traverse in one of the garnets (garnet 1a) previously analyzed by Clechenko and Valley (2003) collected from the Willsboro Mine, NY, USA (approx. 44˚18’52”N, 73˚52’54”W) in order to assess the accuracy of our correction technique, as well as to search for finer-scale isotopic zoning and

possibly larger variation than could be resolved by the existing analyses. The previous laser fluorination data document gradients in $\delta^{18}O$ of ~ 3‰ over 1 mm, but larger and sharper gradients are predicted for contact metamorphism. The new ion microprobe data interrogate these gradients at a scale that is up to 100 times finer in linear resolution and one million times smaller in volume.

6.2 Analysis and correction

The remainder of the polished section of garnet 1a of Clechenko and Valley (2003) was mounted in epoxy with standard *UWG-2* and repolished. The original Fe-Kα X-ray map of the composition of this garnet is reproduced in Figure 5a with the location of the laser-fluorination traverse and the new ion microprobe traverse. The traverse in this study was located adjacent to and parallel with the previous traverse. Seventy ion microprobe analyses were performed along the 7.3 mm transect and corrected to the *UWG-2* standard. The cation composition of the garnet was determined adjacent to each ion microprobe pit by electron microprobe, and used to correct the raw data for bias. The data were corrected using four grossular standards (*GrsSE, 92W-1, 10691, AF749A)* and two intermediate grossular-andradite standards (*92LEW10*, *92LEW7).* The intermediate grossular-andradite standards were analyzed in the same analysis session as the zoned garnet (June 2007) and the four grossular standards were analyzed in a separate session (August 2008). Instrumental biases for both these sessions are reported in Table 2. *92LEW7* was analyzed during both analytical sessions, and its bias relative to *UWG-2* differed by 0.03‰. Although analysis of secondary garnet standards during the same analysis session is desirable, normalization to *UWG-2* allows this correction to be made with a negligible change in estimated precision and accuracy. Ion microprobe analyses of standards, cation compositions for each analysis point,

and the correction scheme used are presented in Table D and Figure B, electronic supplementary materials.

6.3 Results and Discussion

The andradite composition of garnet 1a is plotted versus distance from the garnet rim in Figure 5b. The overall pattern of chemical composition is almost identical to the traverse made by Clechenko and Valley (2003, see their Fig. 5a), but was offset ca. 300 μm along strike of the banding. The oxygen isotopic traverse from this study is plotted in Figure 5c, superimposed on the laser fluorination data of Clechenko and Valley (2003).

The oxygen isotope zoning in garnet 1a measured by ion microprobe is quite well correlated with that measured by laser fluorination. Two relatively andradite-rich, high-$\delta^{18}O$ zones are interspersed with andradite-poor, low-$\delta^{18}O$ zones within 7300 μm of the rim (Fig. 5b). The ion microprobe analyses reproduce most of the laser fluorination traverse within the stated uncertainty of the technique. However, ion microprobe analyses of the outermost low-$\delta^{18}O$ zone yield isotope ratios up to 1‰ lower than that determined by the one laser fluorination analysis at 0-1000 μm. Although it is possible that this discrepancy is due to a source of bias that is unaccounted for in the correction scheme, this seems unlikely, especially sine there is no indication of a hydrogrossular component in this sample Other intermediate grossular composition zones in this garnet show close agreement between laser and ion microprobe analyses (e.g., 4500μm from the rim), suggesting that no systematic relationship between grossular and analysis misfit exists. Mixed-composition laser analyses are the most likely explanation for this discrepancy.

Examination of this and similar garnets from Willsboro and related nearby wollastonite skarns shows that the andradite bands parallel euhedral crystal faces of garnet

506 (Clechenko and Valley, 2003). In many cases, zoning is preserved in only parts of the garnet.
507 In Fig. 5a, these bands can be seen to become diffuse 3-5 mm to the left of the analysis
508 traverses because the garnet was sheared and recrystallized during granulite facies
509 metamorphism. Similar recrystallization has affected most of the garnets at Willsboro with
510 the result that their cation compositions are homogenized and that they record Sm-Nd ages
511 reset during regional metamorphism at ca. 1035 Ma (Basu et al. 1988). Taken together, all
512 data support the interpretation that zoned garnets formed at the time of contact
513 metamorphism and were locally preserved in low strain zones during recrystallization ca. 100
514 myr later. The sharp chemical zonation that parallels garnet crystal faces (Fig.5a) resulted
515 from growth zoning at 1155 Ma and is texturally and chemically distinct from the more
516 diffuse effects of granulite facies recrystallization .

517 In the unrecrystallized domains of garnet 1a, BSE imaging and electron microprobe
518 analyses reveal oscillatory zonation in Al and Fe^{3+} but not the multiple μm-scale oscillations
519 characteristic of many skarn garnets. Ion microprobe analysis of oxygen isotope ratios in this
520 garnet reveals a generally smooth profile with only two sharp changes in isotopic
521 composition (~1400 and ~5500 μm from the garnet edge). One possible reason for the
522 absence of μm-scale features is diffusional relaxation of chemical and isotopic gradients
523 during the granulite-facies regional metamorphic overprint. Clechenko and Valley (2003)
524 calculated a characteristic length scale of diffusion (distance over which 50% exchange is
525 predicted to have taken place) of 60 μm for oxygen in the Willsboro garnets based on the
526 experiments of Coghlan (1990) and a thermal event of 750˚C for 50 My, based on regional
527 thermobarometry and geochronology (Bohlen et al., 1985; McLelland et al., 2001). This
528 length-scale of homogenization is consistent with the data-set of Clechenko and Valley

529 (2003) and suggests that fine-scale chemical features were homogenized in the Willsboro
530 garnets, and only mm-scale zonation was preserved through granulite-facies metamorphism.
531 The most important feature of the new ion microprobe data for $\delta^{18}O$ is the sharp
532 gradient between the outermost low-$\delta^{18}O$ rim and high-$\delta^{18}O$ zone between 1377 to 1393 μm
533 from the edge of the garnet (Fig. 5c). This transition represents a jump of 2.1‰ in 16 μm
534 (measured from the center of the analysis pits) coincident with an equally sharp change in the
535 andradite content of garnet visible in the back-scattered electron image in Figure 6a.
536 Although $\delta^{18}O$ decreases gradually across the Fe-rich band from a maximum of 6.3‰ at
537 2400μm to 4.2 ‰ at 1400μm, the oxygen isotope ratios measured in the outermost grossular-
538 rich zone are constant at 1.8‰ (Fig. 5c). If the gradual decrease in $\delta^{18}O$ within the more
539 andradite-rich band were the result of diffusional relaxation after garnet growth across an
540 original step-change in $\delta^{18}O$ at 1380 μm, a symmetrical increase in $\delta^{18}O$ would occur in the
541 adjacent grossular-rich zone approaching 1380 μm. No gradual change is seen from 500 to
542 1380 μm and thus the smooth changes in $\delta^{18}O$ within the andradite-rich band are interpreted
543 as growth-zoning, as is the sharp 2.1‰ gradient at 1380μm between these two zones.
544 The preservation of a sharp gradient in ™^{18}O at 1380 ⌠m provides a very tight constraint on
545 the maximum amount of oxygen diffusion in this garnet throughout its entire history. There
546 is no diffusional process that would sharpen a $\delta^{18}O$ gradient, once formed. Thus, the
547 maximum amount of oxygen exchange can be estimated if the gradient is assumed to have
548 formed as a step of 2.1‰ over 0μm. This is a boundary condition, and it is possible that
549 garnet growth produced a more gradual profile, closer to that observed in this garnet. If this
550 were the case, models based on an initial step condition will over-estimate the duration of the
551 metamorphic event or rate of exchange.

552 Diffusion of oxygen across this boundary was modeled as a simple, 1-dimensional
553 system using equation 3.45 of Crank (1975). Because of the small scale of diffusion (<
554 16μm) compared to the size of the garnet (> 1 cm), the 1-D model is a conservative
555 approximation. Initial values for core and rim $\delta^{18}O$ were taken as the average of ion
556 microprobe data within 100 μm of the transition (4.3±0.4‰ and 1.8±0.5‰, respectively).
557 The sharp Fe^{3+}/Al and $\delta^{18}O$ transition boundary at 1380 ⌈m is shown in back-scattered
558 electron imaging in Figure 6a and analysis pits are labeled in $\delta^{18}O$ VSMOW. A detail of the
559 ion-microprobe traverse in this region is shown in Figure 6b with modeled diffusion curves
560 superimposed on the data. At 750˚C, the diffusion rate (D) of oxygen in garnet based the
561 experiments of Coghlan (1990, P_{H2O} = l kbar) is estimated at $4.2x10^{-25} m^2 s^{-1}$. At this rate, the
562 observed step could only have survived a thermal event of less than 1 My. Furthermore, this
563 calculation does not include the effects of diffusion that would have also occurred during the
564 heating and cooling of regional metamorphism. The extremely rapid heating and cooling
565 required by the sharp gradient in this garnet interpreted in the context of the experiments of
566 Coghlan (1990) are in striking contrast to the slow cooling rates of ~ 1.5˚C/My reported by
567 Mezger et al. (1991) for this region. Although fleeting thermal events have recently been
568 proposed for regional metamorphism (e.g., Ague and Baxter, 2007), it seems unlikely that the
569 mid-crustal, 7-8 Kb granulite-facies regional metamorphism of the Adirondack Highlands
570 could have taken place over so short a time span. Coghlan (1990) reports a conservative error
571 envelope for the diffusion coefficient used in this calculation and even at the extreme, the
572 slowest value of D within this range (i.e., the lowest value of D_o and the highest value of E_A)
573 is not consistent with a peak of metamorphism lasting as long as 50 Myr. Taken together, the
574 experimental data and the measured gradient for $\delta^{18}O$ (Fig. 6b) are most consistent with a

575 thermal peak lasting less than 5 My. If these estimates of the diffusion rate of oxygen in
576 garnet at 750^{o}C are correct, then the peak of regional metamorphism in the NE Adirondack
577 Highlands was significantly faster than has previously been assumed. With increased
578 understanding of the diffusion rate of oxygen in garnet and with further ion microprobe
579 studies of single crystals, time and rate estimates based on oxygen diffusion profiles in garnet
580 (and other minerals) will become more accurate than presently possible.

581 New technology and techniques used in the analysis of oxygen isotopes by ion
582 microprobe have greatly improved the precision of the technique in the analysis of phases
583 with limited solid solution. The use of a single garnet standard mounted in samples, regularly
584 analyzed as a monitor for changes in instrumental conditions, provides similar precision in
585 the analysis of garnets. The correction of instrumental bias due to cation composition in
586 garnets can be done readily using 3 or more compositional standards in a separate standard
587 mount. A correction scheme based on the grossular content of pyralspite garnets and the
588 andradite content of ugrandite garnets brings the accuracy of analyses to the same order as
589 analytical precision with a combined uncertainty of ± 0.5 to 0.6‰, 2 S.D. Application of this
590 approach to garnets will have widespread utility for estimation of thermal and fluid history
591 during metamorphism.

592

593 **Acknowledgements**. This research was begun while FZP was a post-doctoral fellow
594 at the University of Wisconsin supported by (NSF-EAR 0509639). The authors thank Mike
595 Spicuzza for laser fluorination analyses of δ^{18}O, John Fournelle for assistance in electron
596 microprobe analysis and SEM imaging, Brian Hess for sample preparation, and Bin Fu,
597 Penny Lancaster, and Taka Ushikubo for helpful conversations. Dan Schulze, Daniel

598 Vielzeuf, Matt Kohn, Lee Riciputi, John Eiler, Colin Graham, Steve Elphick, and John
599 Craven provided garnet samples. The acquisition of the SEM at Oberlin College used in this
600 study was supported by NSF-EAR 02xxxx). WiscSIMS is partly supported by NSF-EAR
601 (0319230, 0744079), DOE (93ER14389).
602

603

604

605 **References**

606 Afifi, A.M. and Essene, E.J. (1988) Minfile: a microcomputer program for storage and
607 manipulation of chemical data on minerals. Am. Mineral., 73: 446-448.
608 Ague, J.J. and Baxter, E.F. (2007) Brief thermal pulses during mountain building recorded by
609 Sr diffusion in apatite and multicomponent diffusion in garnet. Earth and Planet. Sci.
610 Lett., 261: 500-516
611 Basu, A.R., Faggert, B.E., and Sharma, M., 1988. Sm-Nd isotopic study of wollastonite
612 skarn and garnet amphibolite metamorphism in the Adirondack Mountains, New
613 York. *EOS*, 69: 468.
614 Bohlen, S.R., Valley, J.W. and Essene, E.J., 1985. Metamorphism in the Adirondacks: I,
615 Petrology, pressure and temperature. J. Pet., 26(4): 971-992.
616 Bowman, J.R., 1998. Stable-isotope systematics of skarns. In: D.R. Lentz, Editor,
617 Mineralized Intrusion-Related Skarn Systems, Mineral. Assoc. Can. Short Course
618 Vol. 26, Mineralogical Association of Canada: 99–145.
619 Cavosie, A.J., Valley, J.W., Wilde, S.A. and EIMF, 2005. Magmatic $\delta^{18}O$ in 4400-3900 Ma
620 detrital zircons: A record of the alteration and recycling of crust in the Early Archean.
621 Earth Plan. Sci. Lett., 235: 663-81.
622 Clechenko, C.C. and Valley, J.W., 2003. Oscillatory zoning in garnet from the Willsboro
623 wollastonite skarn, Adirondack Mts, New York: a record of shallow hydrothermal
624 processes preserved in a granulite facies terrane. J. Meta. Geol., 21: 771-784.
625 Coghlan, R. A., 1990. Studies in diffusional transport: Grain boundary transport of oxygen in
626 feldspars, diffusion of oxygen, strontium, and the REE's in garnet, and the thermal
627 histories of granitic intrusions in south-central Maine using oxygen isotopes. PhD
628 Thesis, Brown University. Providence, RI.
629 Crank, J., 1975. The Mathematics of Diffusion. Oxford University Press, New York, 414 pp.
630 Crowe, D.E., Riciputi, L.R., Bezenek, S. and Ignatiev, A., 2001. Oxygen isotope and trace
631 element zoning in hydrothermal garnets: windows into large-scale fluid-flow
632 behavior. Geology, 29: 479-482.
633 Diella, V., Sani, A., Levy, D. and Pavese, A., 2004. High-pressure synchrotron X-ray
634 diffraction study of spessartine and uvarovite: A comparison between different
635 equation of state models. Am. Mineral., 89: 371-376.
636 Donovan, J.J., Kremser, D. and Fournelle, J.H. (Editors), 2007. Probe for Windows User's
637 Guide and Reference, Enterprise Edition, 355 pp.
638 Eiler, J.M., Graham, C.M. and Valley, J.W., 1997. SIMS analysis of oxygen isotopes; matrix
639 effects in complex minerals and glasses. Chem. Geol., 138: 221-244.
640 Elsenheimer, D. and Valley, J.W., 1993. Submillimeter scale zonation of $\delta^{18}O$ in quartz and
641 feldspar, Isle-of-Skye, Scotland. Geochim. Cosmochim. Acta, 57: 3669-3676.
642 Ford, F., 1987. Petrology and geochemistry of xenoliths from the Blaauwbosch kimberlite
643 pipe, R.S.A., Undergraduate Thesis, University of Toronto, Toronto.
644 Garlick, G.D., Macgregor, I.D. and Vogel, D.E., 1971. Oxygen isotope ratios in eclogites
645 from kimberlites. Science, 172: 1025-1027.

646 Gnaser, H., 2008. Isotopic fractionation of sputtered anions: C^- and C_2^-. Nuc. Instr. & Meth.
647 Phys. Res, Sect. B. 266: 37-43.
648 Hervig, R.L., Williams, P., Thomas, R.M., Schauer, S.N. and Steele, I.M., 1992.
649 Microanalysis of oxygen isotopes in insulators by secondary ion mass spectrometry.
650 Int. J. Mass Spectrom. Ion Proc., 120: 45-63.
651 Huberty JM, Kita NT, Heck PR, Kozdon R, Fournelle JH, Xu H and Valley JW (2009)
652 Crystal orientation effects on bias of $\delta^{18}O$ in magnetite by SIMS. Goldschmidt
653 Conference, Geochim. Cosmochim. Acta v.73:13S, A562.
654 Jamtveit, B., Wogelius, R.A. and Fraser, D.G., 1993. Zonation Patterns of Skarn Garnets -
655 Records of Hydrothermal System Evolution. Geology, 21: 113-116.
656 Jamtveit, B. and Hervig, R.L., 1994. Constraints on transport and kinetics in hydrothermal
657 systems from zoned garnet crystals. Science, 263: 505-508.
658 Kelly, J.L., Fu, B., Kita, N.T. and Valley, J.W., 2007. Optically continuous silcrete quartz
659 cements of the St. Peter Sandstone: High precision oxygen isotope analysis by ion
660 microprobe. Geochim. Cosmochim. Acta, 71: 3812-3832.
661 Kita, N.T., Ushikubo, T., Fu, B. and Valley, J.W., 2009 High precision SIMS oxygen isotope
662 analyses and the effect of sample topography. Chem. Geol.,
663 doi:10.1016/j.chemgeo.2009.02.012.
664 Kohn, M.J. and Valley, J.W., 1998. Effects of cation substitutions in garnet and pyroxene on
665 equilibrium oxygen isotope fractionations. J. Meta. Geol., 16: 625-639.
666 Kohn, M.J., Valley, J.W., Elsenheimer, D. and Spicuzza, M.J., 1993. Isotope zoning in garnet
667 and staurolite; evidence for closed-system mineral growth during regional
668 metamorphism. Am. Mineral., 78: 988-1001.
669 Kohn, M.J. and Valley, J.W., 1994. Oxygen isotope constraints on metamorphic fluid flow,
670 Townshend Dam, Vermont, USA. Geochim. Cosmochim. Acta, 58: 5551-5566.
671 Kohn, M.J., Spear, F.S. and Valley, J.W., 1997. Dehydration-melting and fluid recycling
672 during metamorphism: Rangeley Formation, New Hampshire, USA. J. Petrol., 38:
673 1255-1277.
674 Lancaster PJ, Fu B, Page FZ, Kita NT, Bickford ME, Hill BM, McLelland JM, Valley JW
675 (2009) Genesis of metapelitic migmatites in the Adirondack Mts., New York, J Meta
676 Geol, 27: 41-54.
677 McLelland, J., Hamilton, M., Selleck, B., McLelland, J., Walker, D. & Orrell, S., 2001.
678 Zircon U-Pb geochronology of the Ottawan Orogeny, Adirondack Highlands, New
679 York: regional and tectonic implications. Precamb. Res., 109, 39–72.
680 McLelland, J.M., Bickford, M.E., Hill, B.M., Clechenko, C.C., Valley, J.W. and Hamilton,
681 M.A., 2004. Direct dating of Adirondack Massif anorthosite by U-Pb SHRIMP
682 analysis of igneous zircon; implications for AMCG complexes. Geol. Soc. Am. Bull.,
683 116(11-12): 1299-1317.
684 MacGregor, I.D. and Manton, W.I., 1986. Roberts Victor eclogites: Ancient oceanic crust. J.
685 Geophys. Res., 91: 14,063-14,079.
686 Martin, L., Duchêne, S., Deloule, E. and Vanderhaeghe, O., 2006. The isotopic composition
687 of zircon and garnet: A record of the metamorphic history of Naxos, Greece. Lithos,
688 87: 174-192.
689 Mezger, K., Rawnsley, C., Bohlen, S.R. and Hanson, G.N., 1991. U-Pb garnet, sphene,
690 monazite, and rutile ages: Implications for the duration of high grade metamorphism
691 and cooling histories, Adirondack Mts., New York. J. Geol., 99: 415-428.

692 Novak, G. and Gibbs, G.V., 1971. The crystal chemistry of silicate garnets. Am Mineral., 56:
693 791-825.
694 Page, F.Z., Ushikubo, T., Kita, N.T., Riciputi, L.R. and Valley, J.W., 2007. High-precision
695 oxygen isotope analysis of picogram samples reveals 2 µm gradients and slow
696 diffusion in zircon. Am. Mineral., 92: 1772-1775.
697 Peck, W.H. and Valley, J.W., 2004. Quartz-garnet isotope thermometry in the south
698 Adirondack Highlands (Grenville Province, New York). J. Meta. Geol., 22: 763-773.
699 Peck, W.H., Valley, J.W. and Graham, C.M., 2003. Slow oxygen diffusion rates in igneous
700 zircons from metamorphic rocks. Am. Mineral., 88: 1003-1014.
701 Riciputi, L.R. and Paterson, B.A., 1994. High spatial-resolution measurement of O isotope
702 ratios in silicates and carbonates by ion microprobe. Am. Mineral., 79: 1227-1230.
703 Riciputi, L.R., Paterson, B.A. and Ripperdan, R.L., 1998. Measurement of light stable
704 isotope ratios by SIMS:: Matrix effects for oxygen, carbon, and sulfur isotopes in
705 minerals. Int. J. Mass Spectrom., 178: 81-112.
706 Robie, R.A. and Hemingway, B.S., 1995. Thermodynamic properties of minerals and related
707 substances at 298.15 K and 1 bar (10^5 Pascals) pressure and at higher temperatures. B
708 2131, U. S. Geological Survey, Reston.
709 Schulze, D.J., Valley, J.W. and Spicuzza, M.J., 2003. The oxygen isotope composition of
710 mantle eclogites, 8th International Kimberlite Conference, Victoria, B.C.
711 Shimizu, N. and Hart, S.R., 1982. Isotope Fractionation in Secondary Ion Mass-
712 Spectrometry. J. App. Phys. 53: 1303-1311.
713 Skelton, A., Annersten, H. and Valley, J., 2002. $\delta^{18}O$ and yttrium zoning in garnet: time
714 markers for fluid flow? J. Meta. Geol., 20: 457-466.
715 Taylor, B.E. and O'Neil, J.R., 1977. Stable isotope studies of metasomatic Ca-Fe-Al-Si
716 skarns and associated metamorphic and igneous rocks, Osgood Mountains, Nevada.
717 Contrib. Mineral. Petrol., 63: 1-49.
718 Valley, J.W., 1985. Polymetamorphism in the Adirondacks: Wollastonite at contacts of
719 shallowly intruded anorthosite. In: A.C. Tobi and L.R. Touret Jacques (Editors), The
720 Deep Proterozoic Crust in the North Atlantic Provinces. Reidel, Dordrecht, pp. 217-
721 236.
722 Valley, J.W., 1986. Stable isotope geochemistry of metamorphic rocks. In: J.W. Valley, H.P.
723 Taylor and J.R. O'Neil (Editors), Stable isotopes in high temperature geological
724 processes. Rev. Mineral., Vol. 16, pp. 445-489.
725 Valley J.W. and Kita N.T. (2009) *In situ* Oxygen Isotope Geochemistry by Ion Microprobe,
726 In: Fayek M. (ed) GAC/MAC Short Course: Secondary Ion Mass Spectrometry in the
727 Earth and Planetary Sciences, 41:19-63.
728 Valley, J.W. and Graham, C.M., 1991. Ion microprobe analysis of oxygen isotope ratios in
729 granulite facies magnetites; diffusive exchange as a guide to cooling history. Contrib.
730 Mineral. Petrol., 109: 38-52.
731 Valley, J.W. and O'Neil, J.R., 1982. Oxygen isotope evidence for shallow emplacement of
732 Adirondack anorthosite. Nature, 300: 497-500.
733 Valley, J.W., Bohlen, S.R., Essene, E.J. and Lamb, W., 1990. Metamorphism in the
734 Adirondacks: II, The role of fluids. J. Petrol., 31(3): 555-596.
735 Valley, J.W., Kitchen, N., Kohn, M.J., Niendorf, C.R. and Spicuzza, M.J., 1995. UWG-2, a
736 garnet standard for oxygen isotope ratios: strategies for high precision and accuracy
737 with laser heating. Geochim. Cosmochim. Acta, 59: 5223-5231.

738 Vielzeuf, D., Champenois, M., Valley, J.W., Brunet, F. and Devidal, J.L., 2005a. SIMS
739 analyses of oxygen isotopes: Matrix effects in Fe-Mg-Ca garnets. Chem. Geol., 223:
740 208-226.
741 Vielzeuf, D., Veschambre, M. and Brunet, F., 2005b. Oxygen isotope heterogeneities and
742 diffusional profiles in composite metamorphic/magmatic garnets from the Pyrenees.
743 Am. Mineral., 90: 463-472.
744 Yardley, B.W.D., Rochelle, C.A., Barnicoat, A.C. and Lloyd, G.E., 1991. Oscillatory zoning
745 in metamorphic minerals - an indicator of infiltration metasomatism. Mineral. Mag.,
746 55: 357-365.
747
748 **Figure Captions**
749
750 Figure 1. Cation compositions of garnet standards used in this study. Standards used in
751 previous studies are keyed to the study of their first use.
752
753 Figure 2. Instrument bias for oxygen isotope analysis at WiscSIMS (‰ relative to UWG-2)
754 as a function of cation composition of garnet standards expressed in terms of mol %
755 garnet end-members. (a) Bias in Al-rich Mg-Fe^{2+}-Ca-Mn garnets is correlated with
756 grossular content (CaAl). (b) Bias in Ca- rich Al-Fe^{3+} garnets is inversely correlated
757 with grossular. MexGrs is poorly calibrated, see text.
758
759 Figure 3. Instrument bias for oxygen isotope analysis at WiscSIMS ($\delta^{18}O$, ‰ relative to
760 UWG-2) as a function of calculated molar volume of the garnet standards. Errors are
761 plotted as 2 S.E. The line is a least-squares linear regression (equation 5.1) and yields
762 an R^2 value of 0.95. Two garnets (*MexGrs* and *SpsSE*) fall outside of 2 S.E. of the
763 estimate.
764
765 Figure 4. Instrument bias for oxygen isotope analysis at WiscSIMS ($\delta^{18}O$, ‰ relative to
766 UWG-2) as a function of Ca-rich garnet end-members. Instrumental bias in Al-rich
767 pyralspite garnets (plotted as open circles) increases with grossular + uvarovite
768 content. Instrumental bias in Ca-rich ugrandite garnets (plotted as filled circles) is
769 greater than that in pyralspite garnets and increases with andradite + CaTi garnet
770 content. Sample *MexGrs* is poorly calibrated, see text. Error bars are 2 S.E. of
771 multiple analyses and are smaller than the sample points in most cases. The low-
772 andradite grossular sample *GrsSE* appears in both plots. The polynomial best fit
773 curves (equations 5.2 and 5.3) are also shown.
774
775 Figure 5. Oscillatory-zoned skarn garnet from the granulite-facies Willsboro wollastonite
776 skarn, Adirondack Mountains, New York, USA. (a) Fe-Kα X-ray image of the garnet
777 showing andradite-rich zones (purple) and grossular-rich zones (blue). Yellow and
778 orange minerals are sphene and feldspar. The location of the $\delta^{18}O$ analyses by laser
779 fluorination (Clechenko and Valley, 2003) are shown as a thick black line, the
780 location of the ion microprobe traverse in this study is shown as a thick white line. (b)
781 mol % andradite determined by electron microprobe vs. distance from garnet edge
782 (top of figure). (c) traverses of $\delta^{18}O$, open symbols represent ion microprobe analyses
783 with ± 0.6‰ error bars that represent both the precision and accuracy of the

technique, black bars are the laser fluorination data of mg-size samples by Clechenko and Valley (2003).

Figure 6. Sharp $\delta^{18}O$ and cation discontinuity 1377 μm from the garnet edge (a) High-contrast back-scattered electron image of the sharp andradite-grossular transition within the garnet. Ion microprobe pits (10 μm dia.) are labeled with $\delta^{18}O$ ‰ VSMOW. (b) detail of $\delta^{18}O$ traverse over the same field of view with simulated diffusion profiles (see text).

Figure 1

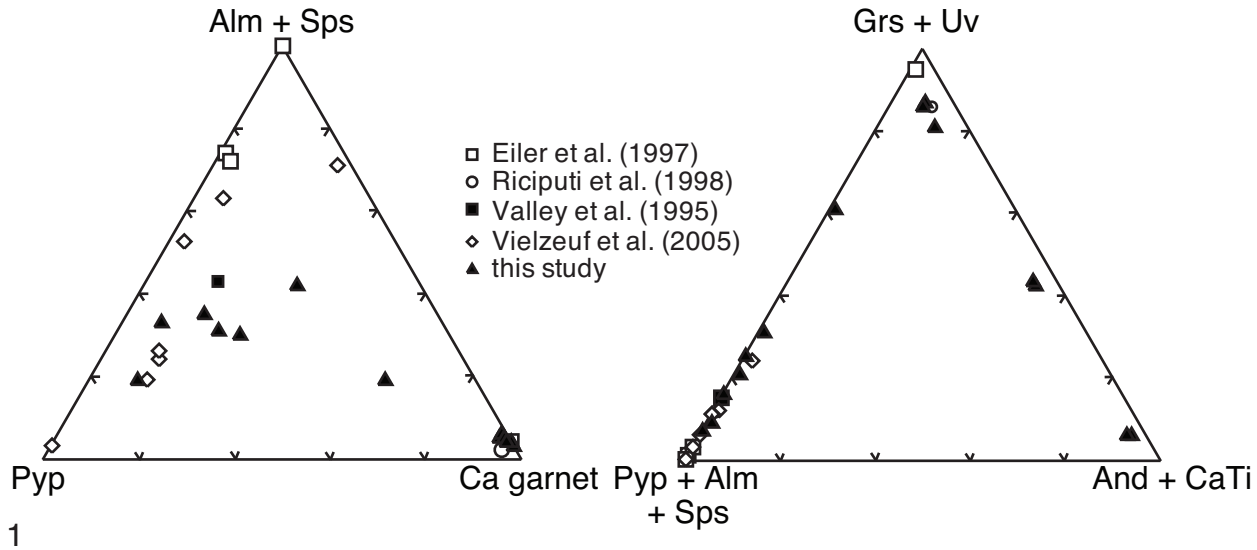

Fig. 1

Figure 2

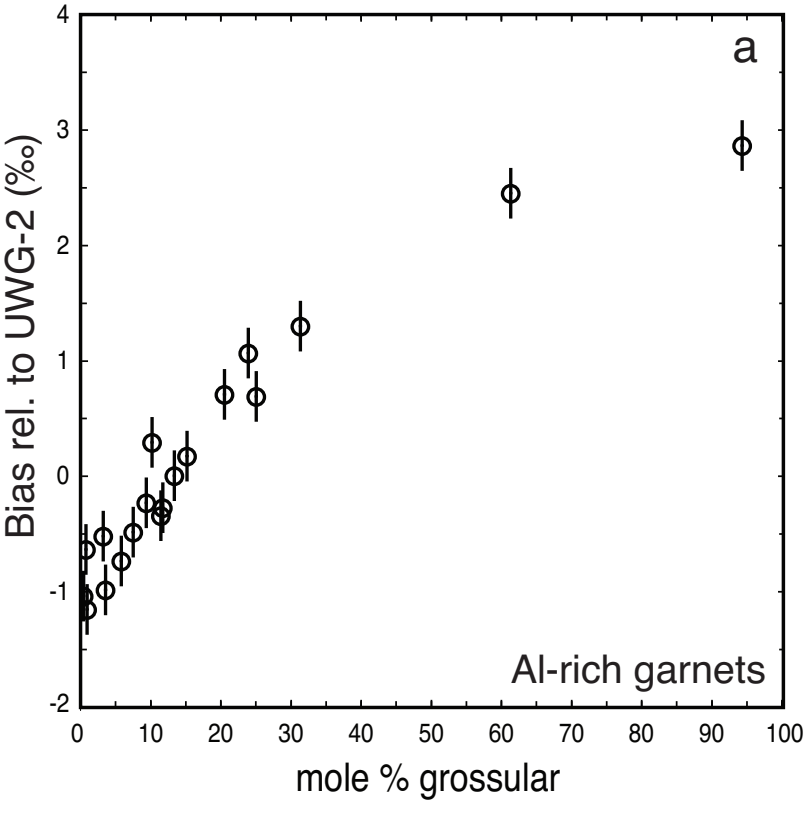
a
Bias rel. to UWG-2 (‰)
mole % grossular
Al-rich garnets

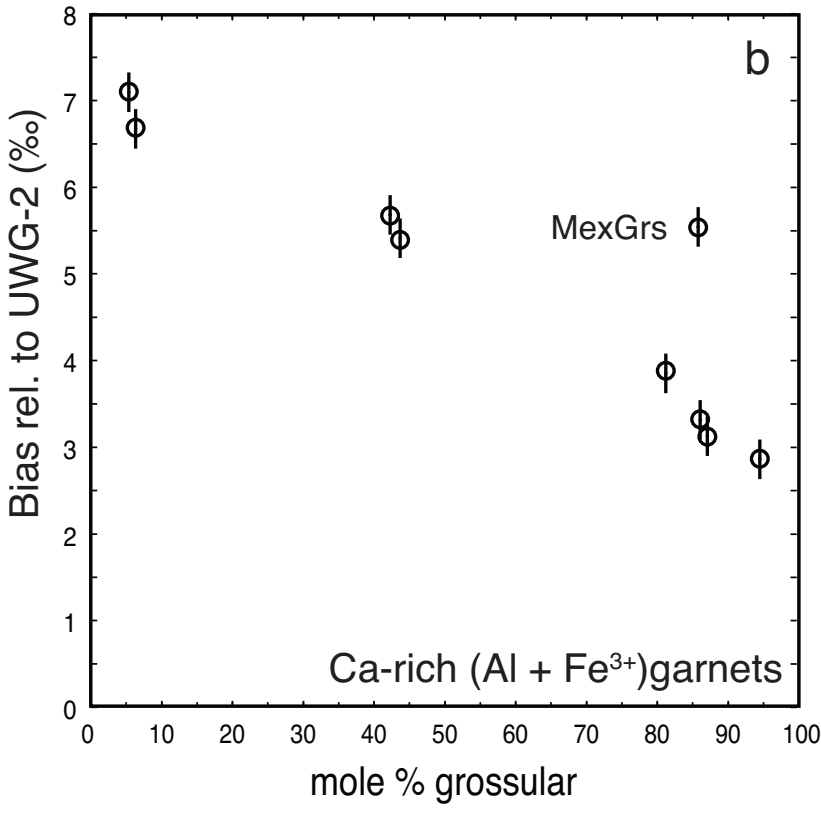
b
Bias rel. to UWG-2 (‰)
mole % grossular
MexGrs
Ca-rich (Al + Fe3+)garnets

Figure 3

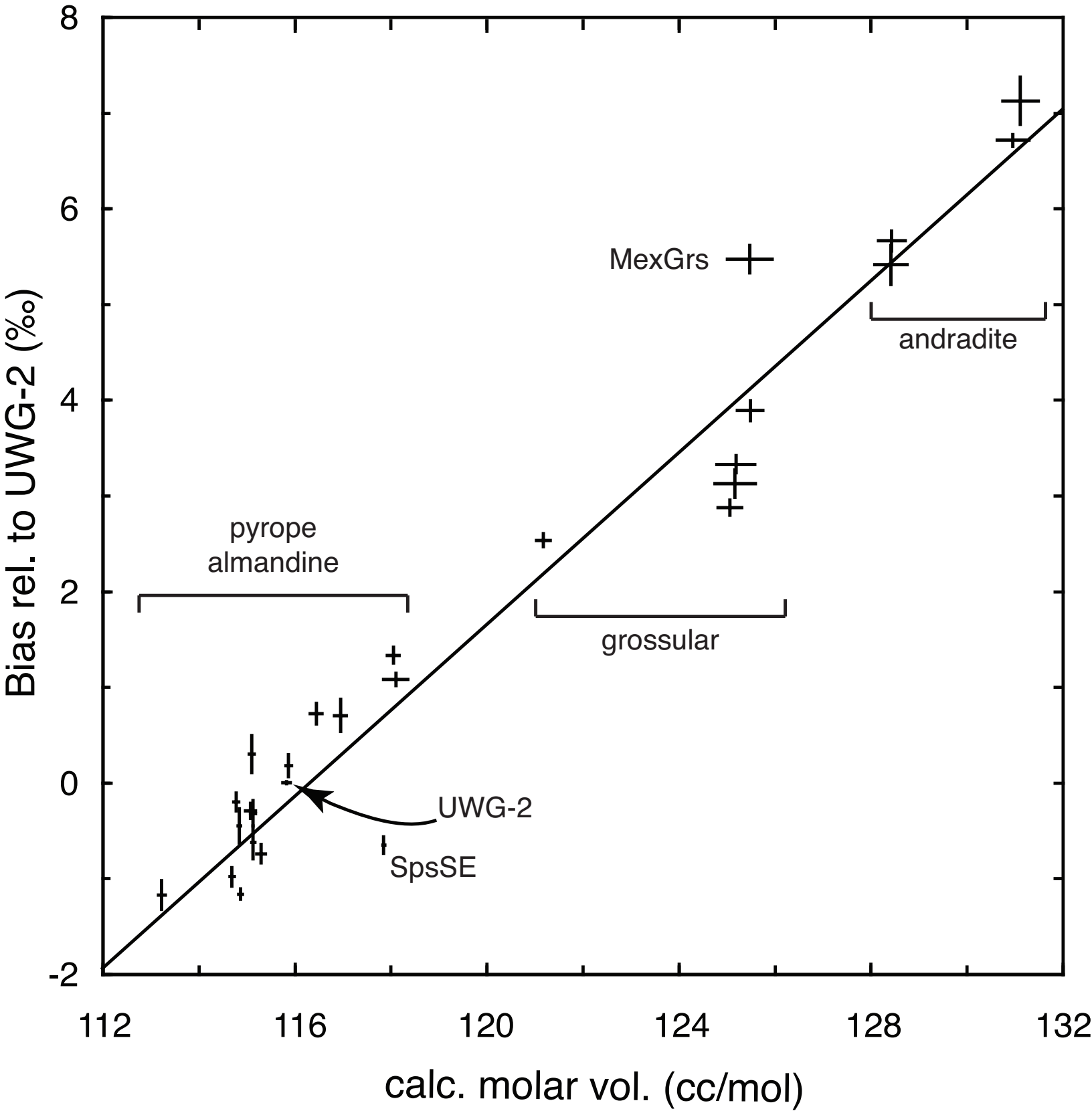
8
6
4
2
0
-2
112
116
120
124
128
132
Bias rel. to UWG-2 (‰)
calc. molar vol. (cc/mol)
MexGrs
andradite
pyrope
almandine
grossular
UWG-2
SpsSE

Figure 4

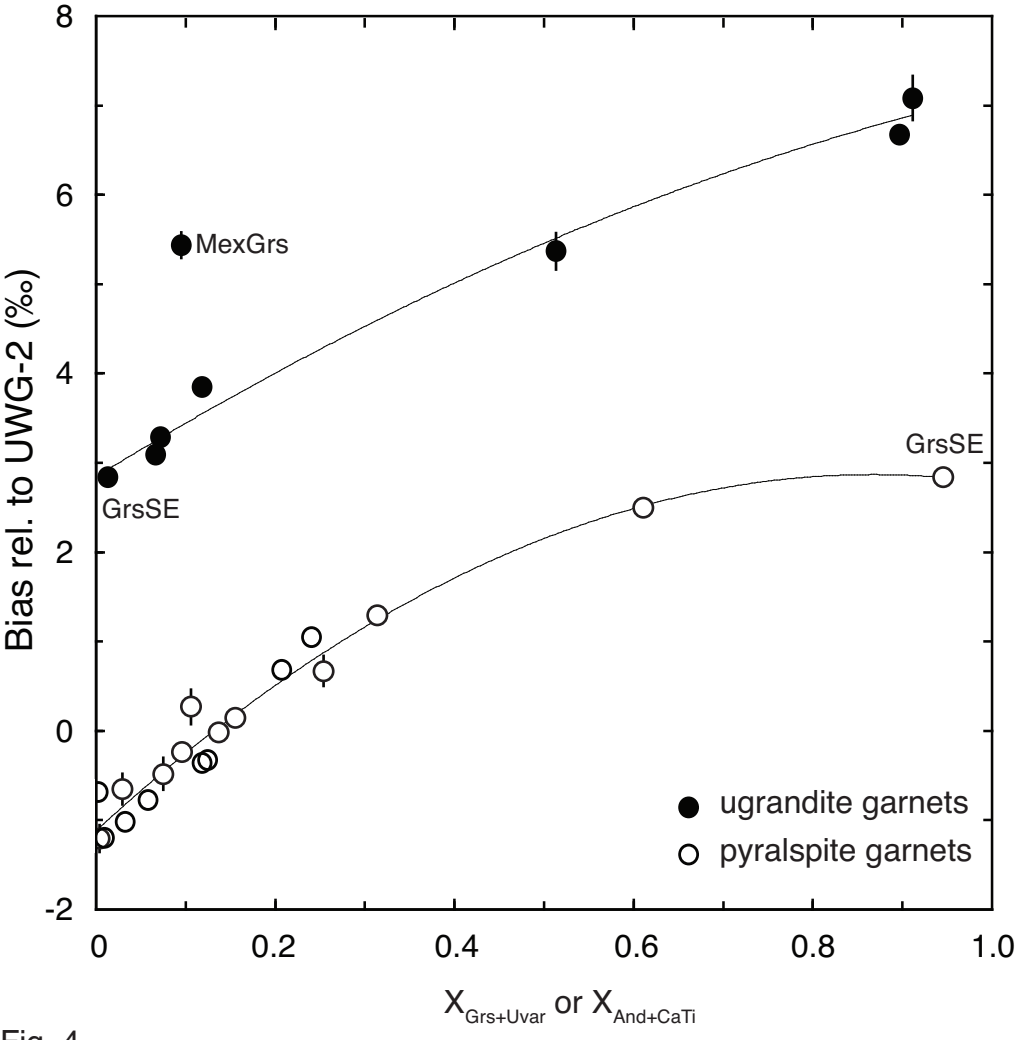

Fig. 4

Figure 5

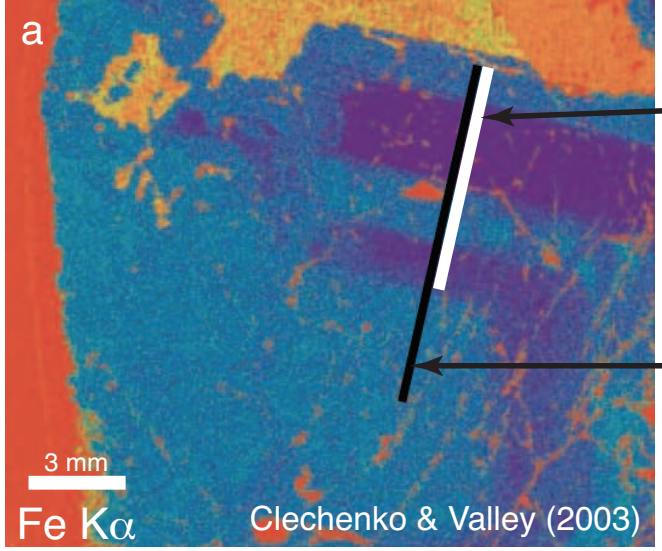

Location of electron- and ion-microprobe traverses shown in (b) and (c).

Location of the laser fluorination $\delta^{18}O$ traverse made by Clechenko & Valley (2003). Data collected immediately adjacent to the traverse made in this study is shown in (c).

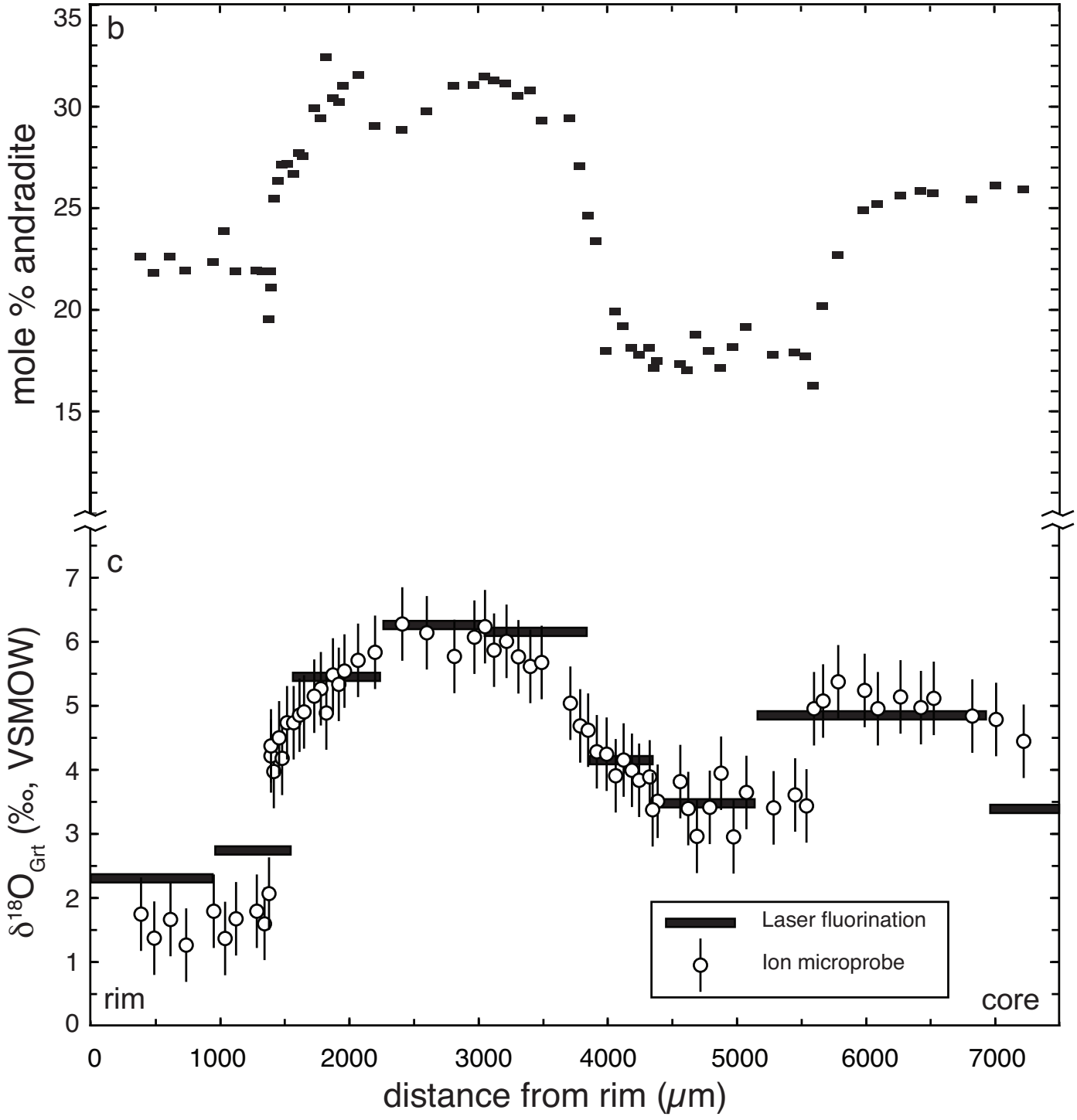

Fig. 5

Figure 6

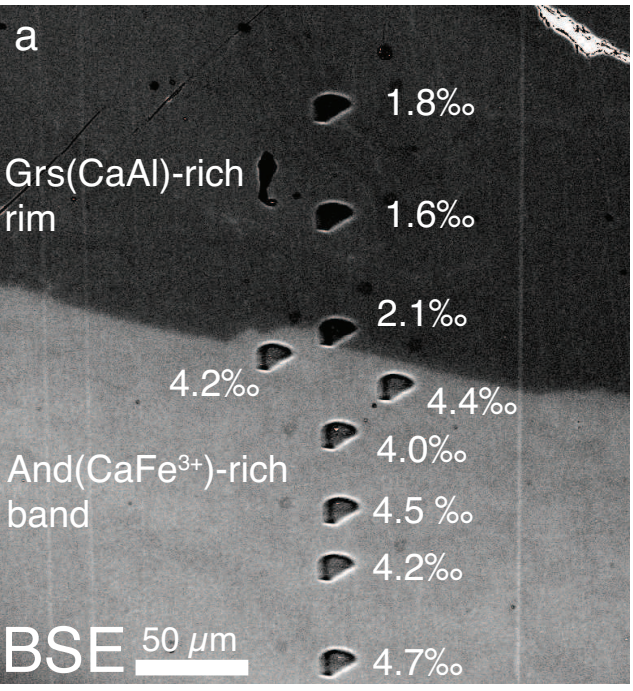

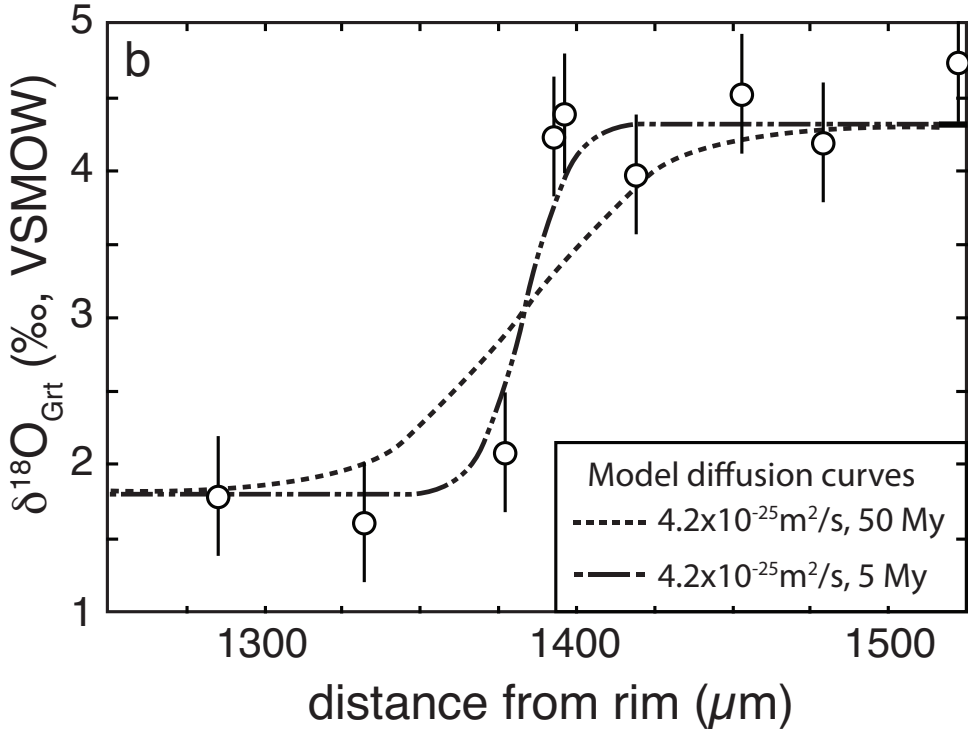

Fig. 6

Table 1

Click here to download Table: Table 1.pdf

Table 1. Garnet standards analyzed for $\delta^{18}O$ at WiscSIMS

Standard	Average composition	Calculated Molar V[1]	2 S.D.[1]	$\delta^{18}O^2$ (‰ VSMOW)	Average[3] $\delta^{18}O$*	Average bias ‰ rel. UWG-2	2 S.D.[4]	n[4]	2 S.E.[4]	Ref.[5]
Pyrope										
PypDM	$Pyp_{97}Alm_3$	113.2	0.07	5.60	4.42	-1.18	0.73	23	0.15	(6)
13-63-19	$Pyp_{71}Alm_{18}Grs_9Sps_2$	114.8	0.05	5.92	5.71	-0.21	0.29	10	0.09	(5)
PypAA	$Pyp_{69}Alm_{18}Grs_{11}Sps_1Uv_1$	115.1	0.10	5.50	5.20	-0.30	0.25	10	0.08	(6)
PypAK	$Pyp_{64}Alm_{24}Grs_{11}Sps_1$	115.1	0.05	5.50	5.17	-0.33	0.42	10	0.13	(6)
PypMM	$Pyp_{63}Alm_{25}Grs_{11}Sps_1$	115.1	0.05	5.30	5.59	0.29	0.60	10	0.19	(6)
13-62-29	$Pyp_{59}Alm_{32}Grs_8Sps_1$	114.9	0.03	7.39	6.93	-0.46	0.56	10	0.18	(5)
13-62-27	$Pyp_{49}Alm_{35}Grs_{15}Sps_1$	115.9	0.06	6.49	6.66	0.17	0.36	10	0.11	(5)
13-63-20	$Pyp_{48}Alm_{31}Grs_{20}Sps_1$	116.5	0.12	6.14	6.85	0.71	0.34	10	0.11	(5)
13-63-44	$Pyp_{45}Alm_{29}Grs_{25}Sps_1$	117.0	0.12	6.37	7.06	0.69	0.53	10	0.17	(5)
Almandine										
AlmSE	$Alm_{74}Pyp_{25}Grs_1$	114.9	0.03	8.30	7.13	-1.17	0.31	38	0.05	(2), (6)
AlmCMG	$Alm_{70}Pyp_{25}Grs_3Sps_2$	115.1	0.03	7.50	6.87	-0.63	0.65	14	0.17	(2), (6)
2B3	$Alm_{67}Grs_{24}Sps_4\,Pyp_3And_2$	118.1	0.26	6.90	7.97	1.07	0.35	30	0.06	(6)
Beta114	$Alm_{61}Pyp_{31}Grs_6Sps_2$	115.3	0.09	9.30	8.55	-0.75	0.45	30	0.08	(6)
Bal509	$Alm_{52}Pyp_{44}Grs_3Sps_1$	114.7	0.04	12.30	11.31	-0.99	0.30	10	0.09	(6)
UWG-2	$Alm_{45}Pyp_{40}Grs_{14}Sps_1$	115.8	0.08	5.80	5.80	0.00	0.35	357	0.02	(1), (2), (6)
13-63-21	$Alm_{41}Grs_{31}Pyp_{27}Sps_1$	118.1	0.12	4.55	5.87	1.32	0.30	14	0.08	(5)
Spessartine										
SpsSE	$Sps_{94}Alm_6$	117.9	0.02	5.40	4.74	-0.66	0.36	19	0.08	(2), (6)
Grossular										
GrsSE	$Grs_{94}Alm_4Sps_1CaTi_1$	125.1	0.24	3.80	6.66	2.86	0.48	37	0.08	(2), (6)
92W-1	$Grs_{87}And_5Alm_5Pyp_2CaTi_1$	125.2	0.42	-0.34	2.77	3.11	0.63	20	0.14	(4)
10691	$Grs_{86}And_5Alm_5Pyp_2CaTi_2$	125.2	0.40	0.18	3.49	3.31	0.28	10	0.09	(4)
MexGrs	$Grs_{86}And_8Pyp_3Alm_1Sps_1CaTi_1$	125.5	0.47	10.60	16.05	5.45	0.67	22	0.14	(3)
AF749A	$Grs_{81}And_{10}Alm_5Pyp_1Sps_1CaTi_2$	125.5	0.26	-1.24	2.63	3.87	0.32	10	0.10	(4)
R-53	$Grs_{61}Alm_{19}Pyp_{19}CaTi_1$	121.2	0.14	5.33	7.85	2.52	0.15	5	0.07	(5)
Andradite										
92LEW2	$And_{91}Grs_6Alm_3$	131.1	0.37	-1.47	5.63	7.10	0.78	10	0.25	(4)
92LEW7	$And_{89}Grs_6Alm_4Pyp_1$	131.0	0.33	-1.60	5.09	6.69	0.25	18	0.06	(4)
92LEW10	$And_{50}Grs_{42}Alm_4CaTi_2Pyp_2$	128.4	0.28	-1.20	4.44	5.64	0.38	14	0.10	(4)
92LEW8	$And_{49}Grs_{43}Alm_4CaTi_3Pyp_1$	128.4	0.34	-0.93	4.46	5.39	0.64	10	0.20	(4)

[1] (cm^3/mol) calculated from compositional data, see text, [2]Values of $\delta^{18}O$ were calibrated against the VSMOW scale using UWG-2 by laser fluorination and gas-source mass spectrometry, see text. [3]Average raw value measured by ion microprobe, corrected to UWG-2, [4]Variability measured by ion probe.

[5] (1) Valley et al. (1995), (2) Eiler et al. (1997), (3) Riciputi et al. (1998), (4) Kohn & Valley (1998), (5) Schulze et al. (2003), (6) Vielzeuf et al. (2005)

Table 2

Click here to download Table: Table 2.pdf

Table 2. Instrument bias of each garnet standard relative to UWG-2 over a 28 month period

	Bias relative to UWG-2 (‰)									
Standard	Apr-06	Aug-06	Sep-06	Nov-06	Jan-07	Apr-07	Jun-07	Aug-08	Avg.	Range
Pyrope										
PypDM	-1.5	-1.1			-0.9	-0.8			-1.1	0.7
13-63-19	-0.2								-0.2	
PypAA	-0.3								-0.3	
PypAK	-0.3								-0.3	
PypMM	0.3								0.3	
13-62-29	-0.5								-0.5	
13-62-27	0.2								0.2	
13-63-20	0.7								0.7	
13-63-44	0.7								0.7	
Almandine										
AlmSE	-1.2	-1.1	-1.2	-1.0	-1.2			-1.2	-1.1	0.2
AlmCMG	-0.5							-0.9	-0.7	0.4
2B3	1.1	1.1	1.0		1.0				1.1	0.2
Beta114	-0.9		-0.7	-0.7	-0.5				-0.7	0.4
Bal509	-1.0								-1.0	
UWG-2	0.0								0.0	
13-63-21	1.3		1.3						1.3	0.0
Spessartine										
SpsSE	-0.7	-0.6			-0.6				-0.6	0.1
Grossular										
GrsSE	2.7	2.8	2.9		2.8	3.2		3.2	2.9	0.5
92W-1								3.1	3.1	
10691								3.3	3.3	
MexGrs	5.6						5.5	5.0	5.4	0.6
AF749A								3.9	3.9	
R-53	2.4	2.5							2.4	0.2
Andradite										
92LEW2	7.1								7.1	
92LEW7	6.7						6.6	6.6	6.7	0.1
92LEW10	5.6						5.7		5.7	0.1
92LEW8	5.4								5.4	